## Supporting Information

# Direct formation of interlayer exciton in two-dimensional van der Waals heterostructures

Xianghong Niu[1], Shanshan Xiao[3], Dazhong Sun[1], Anqi Shi[3], Zhaobo Zhou[2], Wei Chen[1], Xing'ao Li[1,3], Jinlan Wang[2*]

[1] New Energy Technology Engineering Laboratory of Jiangsu Province & School of Science, Nanjing University of Posts and Telecommunications, Nanjing 210023, China
[2] School of Physics, Southeast University, Nanjing 211189, China
[3] Key Laboratory for Organic Electronics and Information Displays & Institute of Advanced Materials (IAM), Jiangsu National Synergistic Innovation Center for Advanced Materials (SICAM), Nanjing University of Posts and Telecommunications, Nanjing 210023, China

*Corresondence to：jlwang@seu.edu.cn

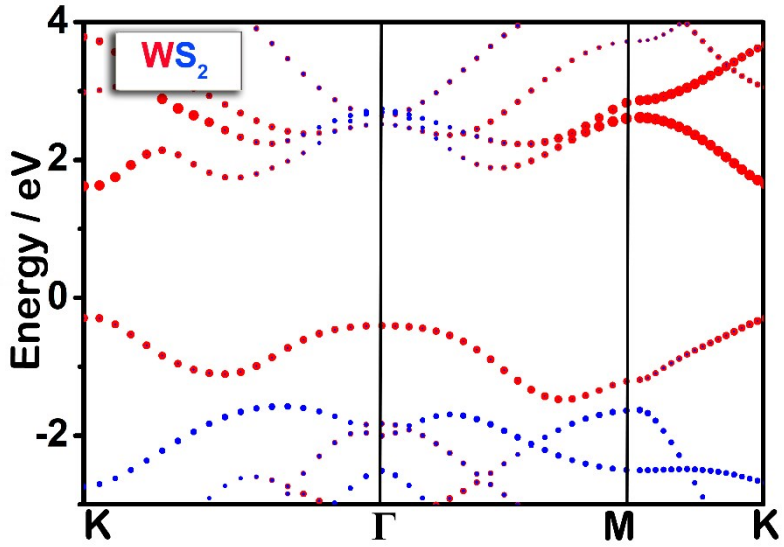


**Figure S1** Projection-resolved band structure of WS. Red and blue indicate the projection onW and S atoms, respectively.

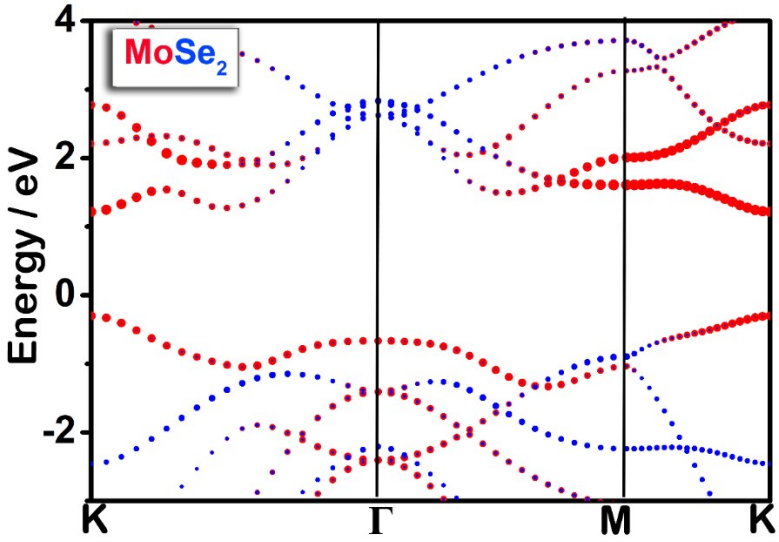


**Figure S2** Projection-resolved band structure of $MoSe_2$. Red and blue indicate the projection on Mo and Se atoms, respectively.

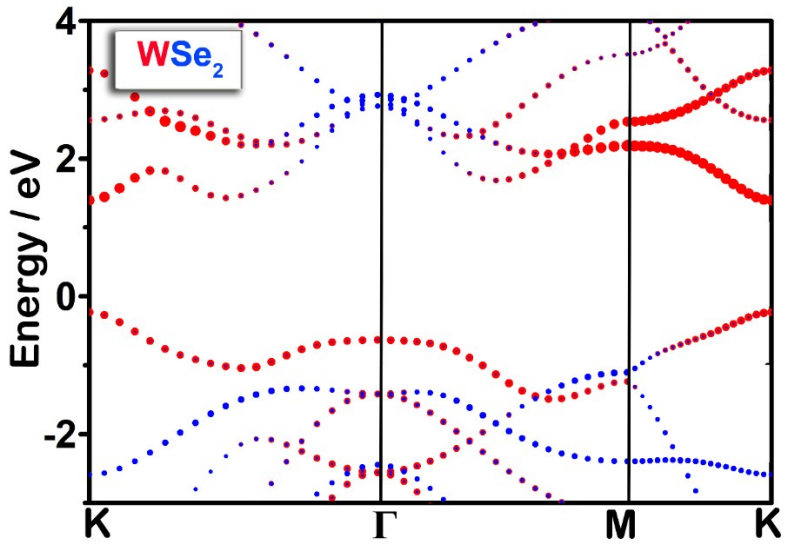


**Figure S3** Projection-resolved band structure of $WSe_2$. Red and blue indicate the projection on W and Se atoms, respectively.

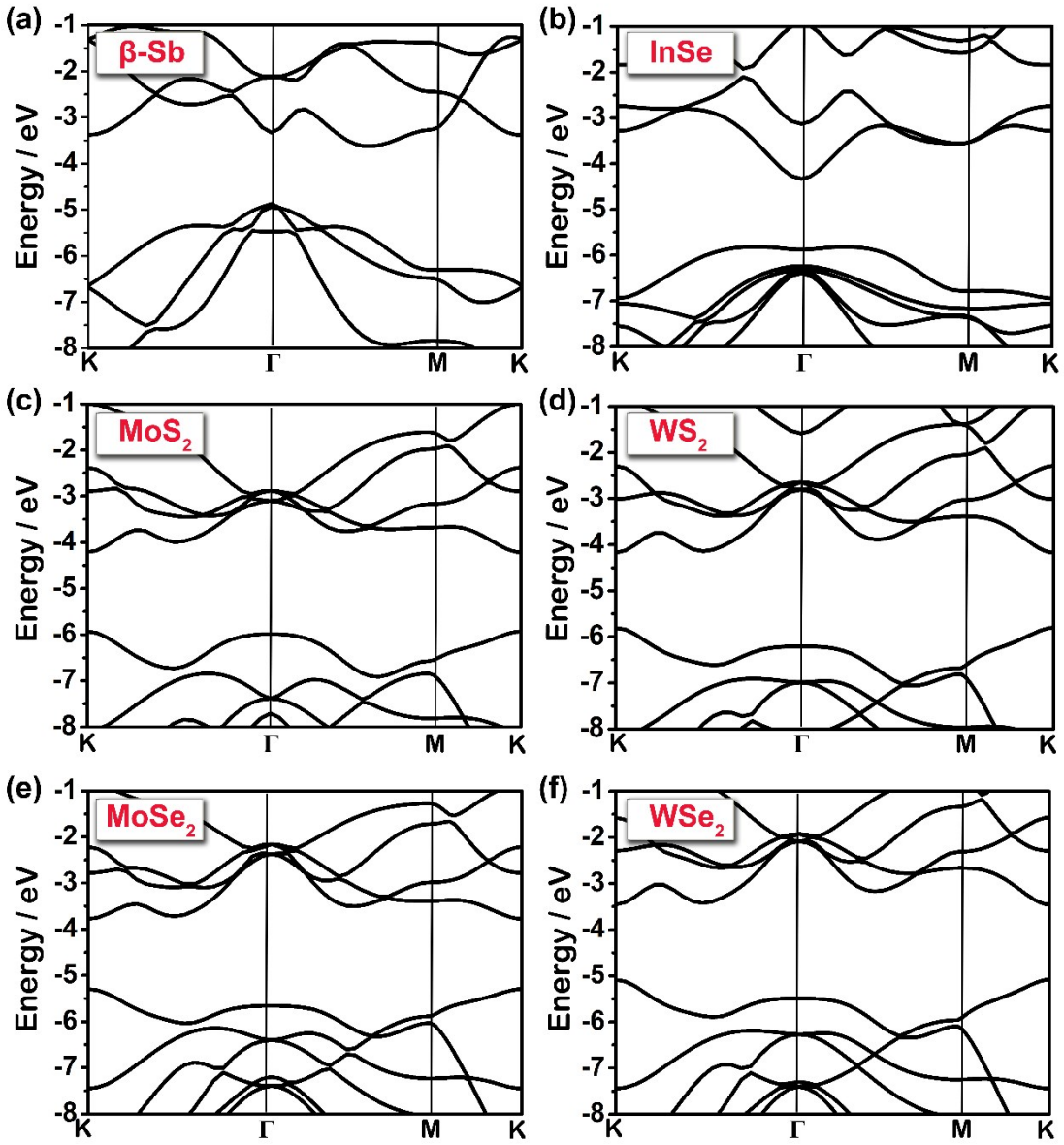


**Figure S4** Band structure of (a) β-Sb, (b) InSe, (c) $MoS_2$, (d) $WS_2$, (e) $MoSe_2$ and (f) $WSe_2$. The energy bands of different systems are aligned to the same vacuum level.

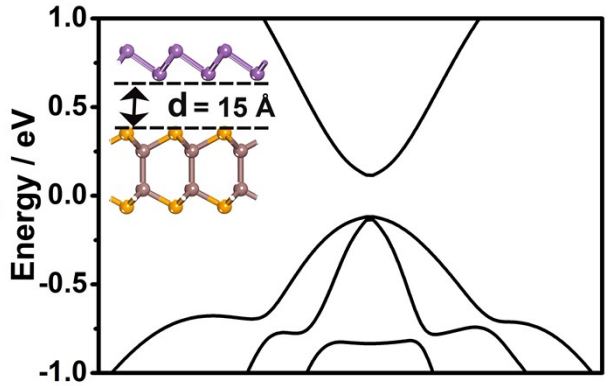


**Figure S5** Electronic structure of InSe/β-Sb heterostructure with interlayer distance of 15 Å. The large interlayer distance indicates that there is no interlayer interaction between InSe and β-Sb layer.

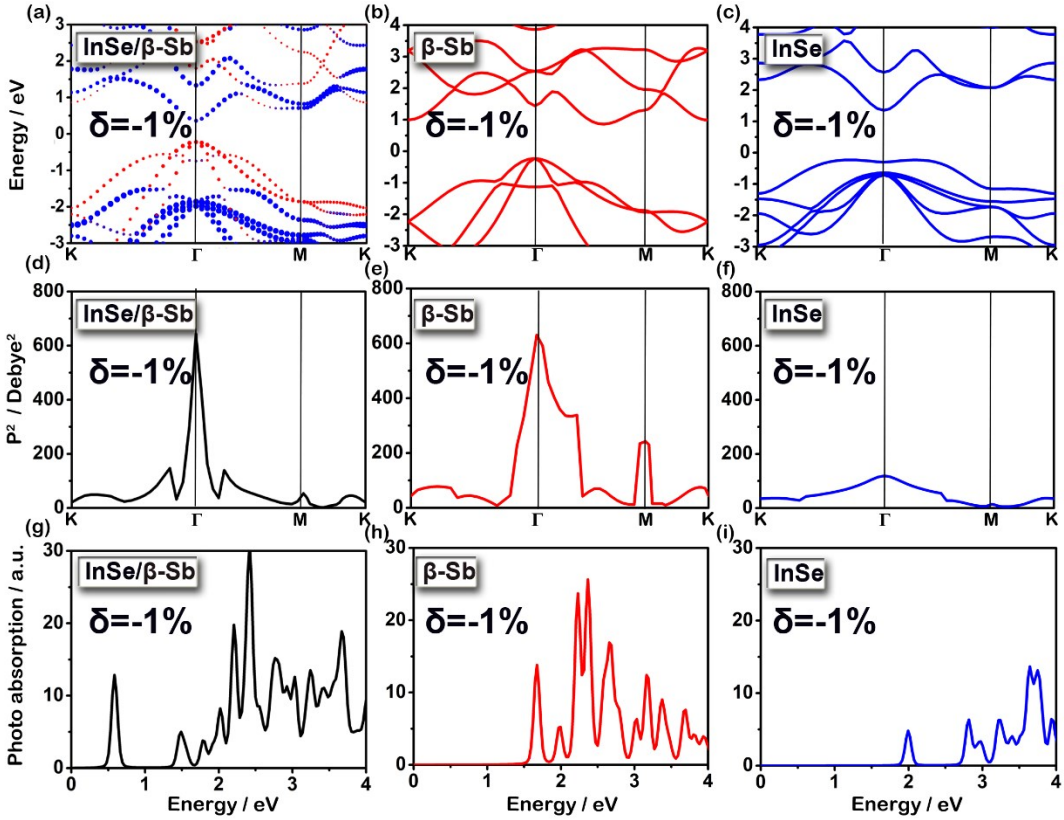


**Figure S6** Under lateral compressive stress -1%: The band structure of (a) InSe/β-Sb heterostructure, (b) β-Sb and (c) InSe sublayer, respectively. The bands plotted in red and blue in (a) denote the bands dominated by β-Sb and InSe layer, respectively. The square of transition dipole moment between the highest valence band and the lowest conduction band for (d) InSe/β-Sb heterostructure, and individual (e) β-Sb, (f) InSe layers, respectively. Photo-absorption properties of (g) InSe/β-Sb heterostructure and individual (h) β-Sb, (i) InSe layers, respectively.

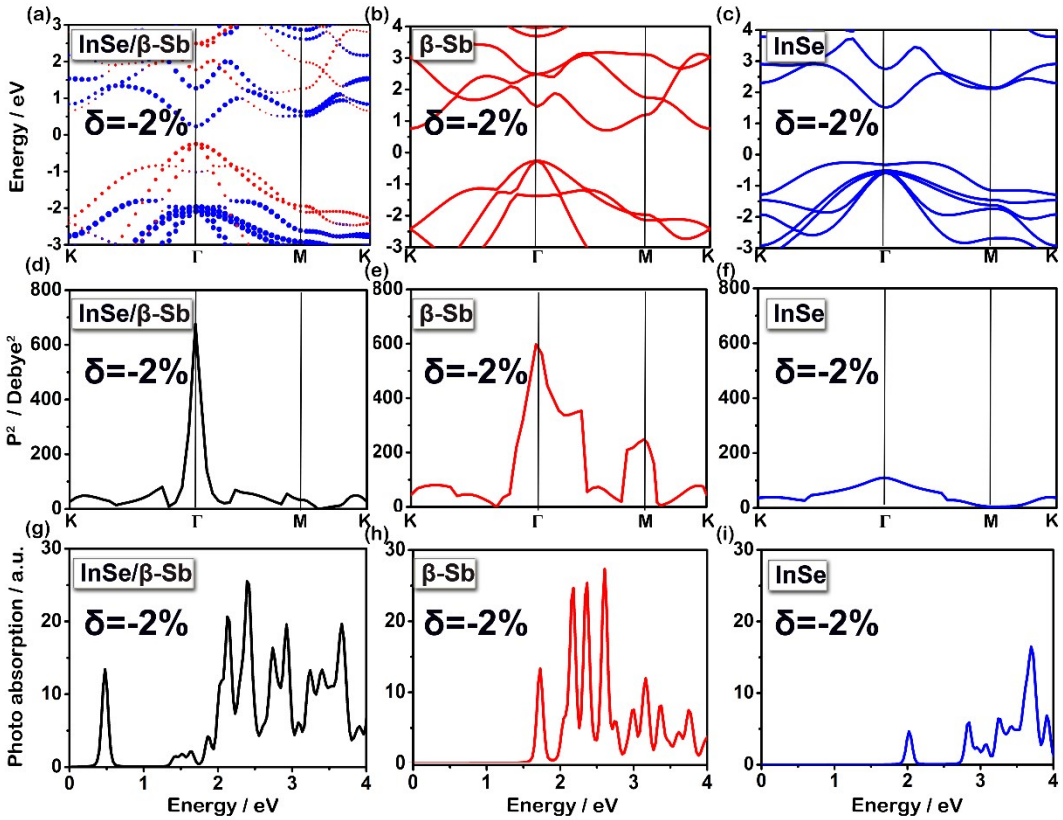


**Figure S7** Under lateral compressive stress -2%: The band structure of (a) InSe/β-Sb heterostructure, (b) β-Sb and (c) InSe sublayer, respectively. The bands plotted in red and blue in (a) denote the bands dominated by β-Sb and InSe layer, respectively. The square of transition dipole moment between the highest valence band and the lowest conduction band for (d) InSe/β-Sb heterostructure, and individual (e) β-Sb, (f) InSe layers, respectively. Photo-absorption properties of (g) InSe/β-Sb heterostructure and individual (h) β-Sb, (i) InSe layers, respectively.

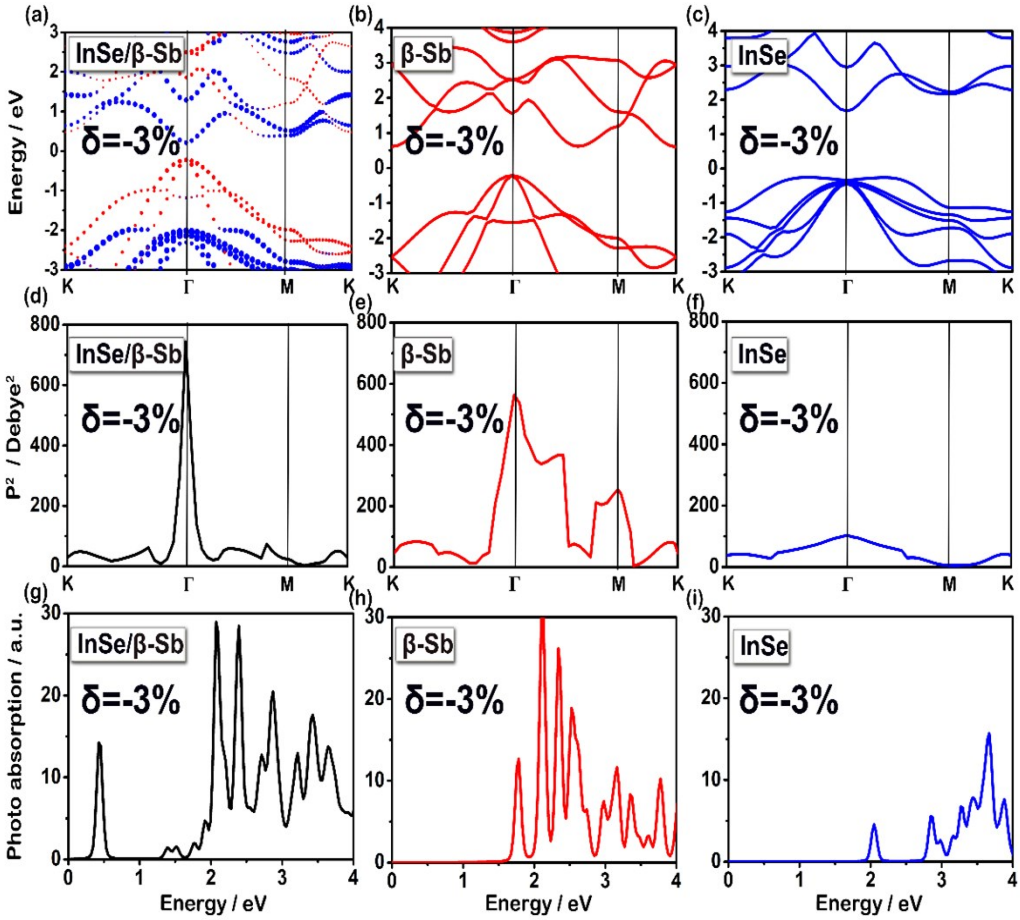


**Figure S8** Under lateral compressive stress -3%: The band structure of (a) InSe/β-Sb heterostructure, (b) β-Sb and (c) InSe sublayer, respectively. The bands plotted in red and blue in (a) denote the bands dominated by β-Sb and InSe layer, respectively. The square of transition dipole moment between the highest valence band and the lowest conduction band for (d) InSe/β-Sb heterostructure, and individual (e) β-Sb, (f) InSe layers, respectively. Photo-absorption properties of (g) InSe/β-Sb heterostructure and individual (h) β-Sb, (i) InSe layers, respectively.

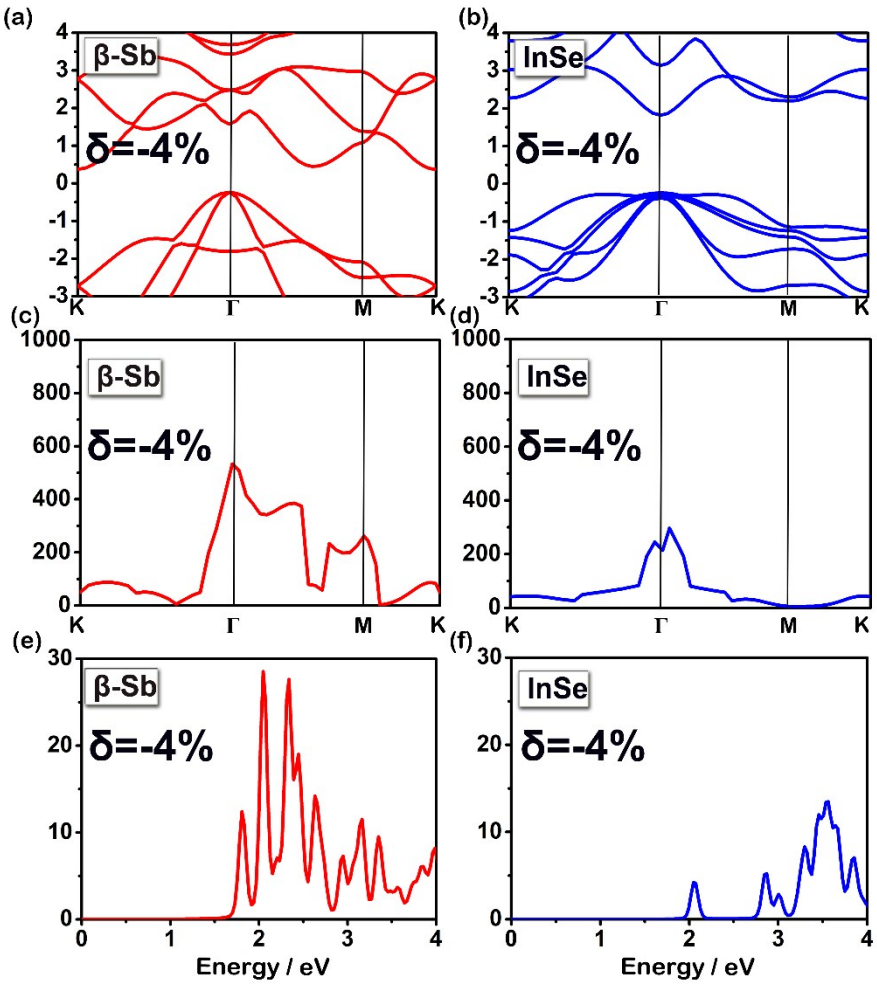


**Figure S9** Under lateral tensile stress -4%: The band structure of (a) β-Sb and (b) InSe sublayer, respectively.. The square of transition dipole moment between the highest valence band and the lowest conduction band for individual (c) β-Sb, (d) InSe layers, respectively. Photo-absorption properties of individual (e) β-Sb, (f) InSe layers, respectively.

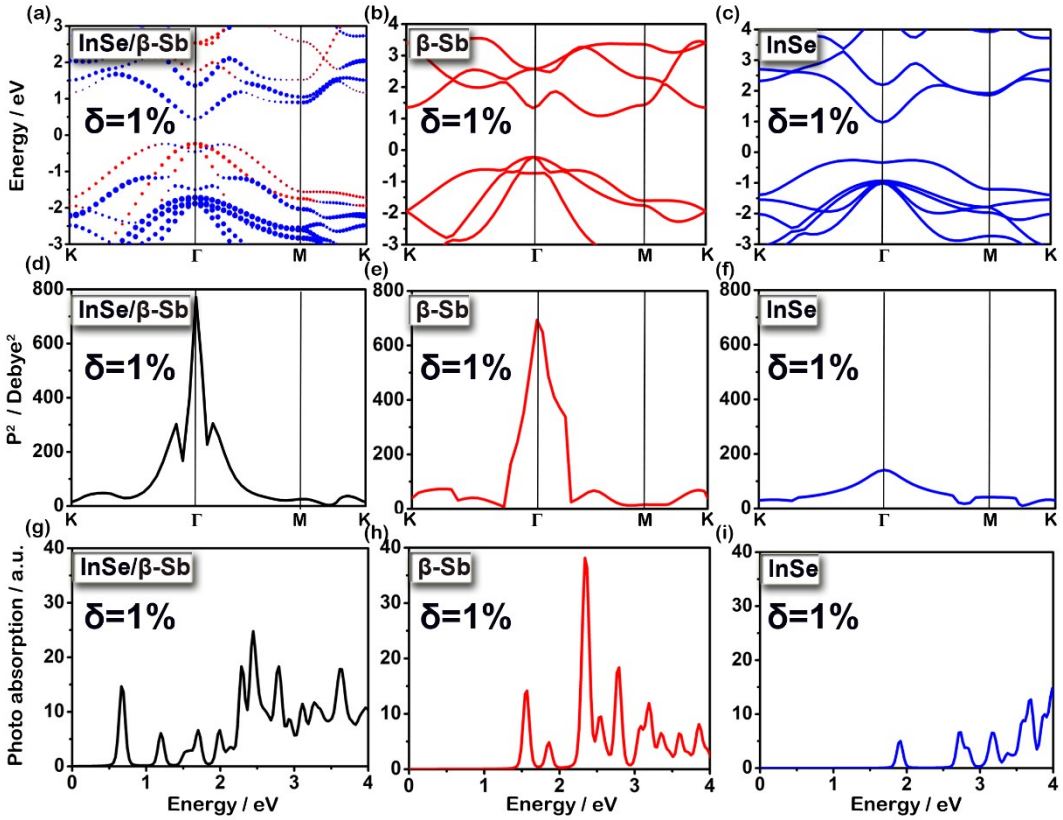


**Figure S10** Under lateral tensile stress 1%: The band structure of (a) InSe/β-Sb heterostructure, (b) β-Sb and (c) InSe sublayer, respectively. The bands plotted in red and blue in (a) denote the bands dominated by β-Sb and InSe layer, respectively. The square of transition dipole moment between the highest valence band and the lowest conduction band for (d) InSe/β-Sb heterostructure, and individual (e) β-Sb, (f) InSe layers, respectively. Photo-absorption properties of (g) InSe/β-Sb heterostructure and individual (h) β-Sb, (i) InSe layers, respectively.

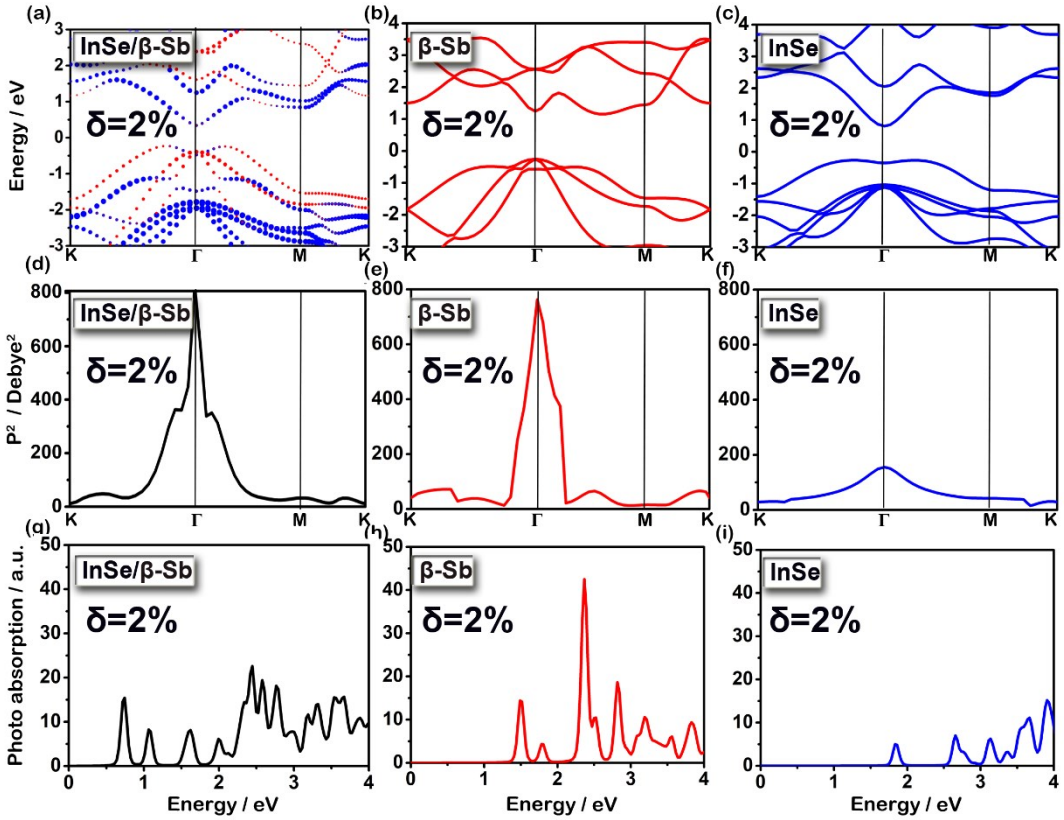


**Figure S11** Under lateral tensile stress 2%: The band structure of (a) InSe/β-Sb heterostructure, (b) β-Sb and (c) InSe sublayer, respectively. The bands plotted in red and blue in (a) denote the bands dominated by β-Sb and InSe layer, respectively. The square of transition dipole moment between the highest valence band and the lowest conduction band for (d) InSe/β-Sb heterostructure, and individual (e) β-Sb, (f) InSe layers, respectively. Photo-absorption properties of (g) InSe/β-Sb heterostructure and individual (h) β-Sb, (i) InSe layers, respectively.

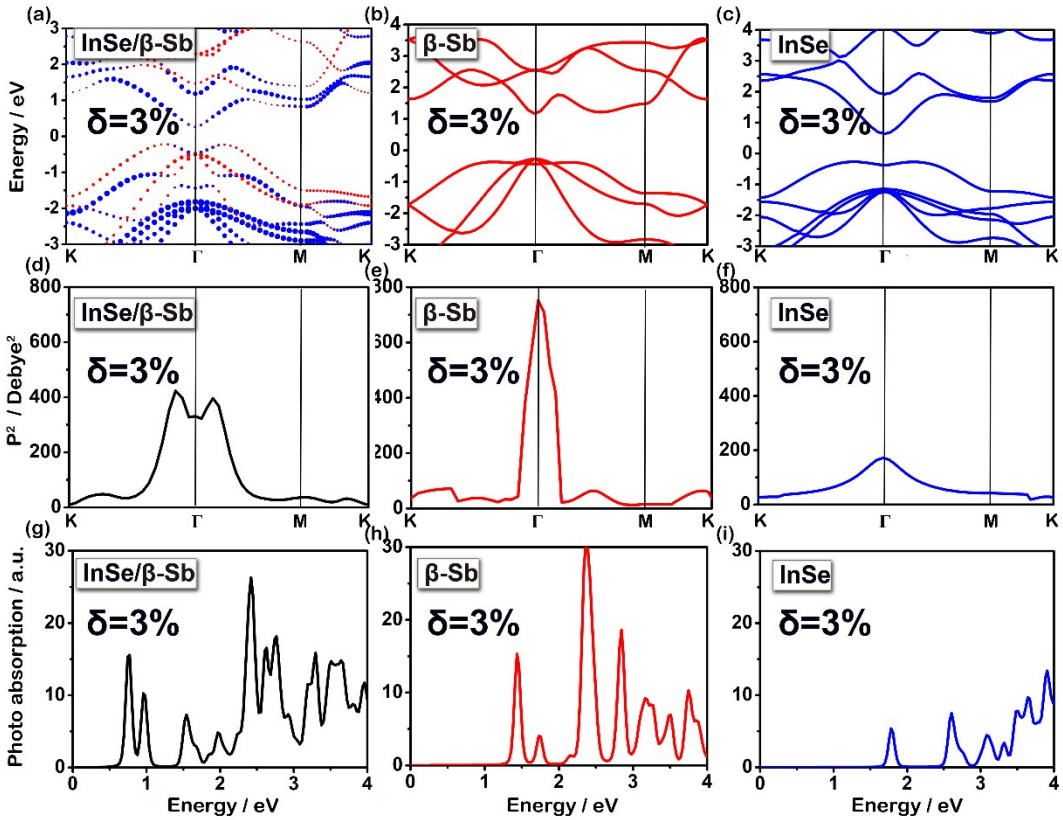


**Figure S12** Under lateral tensile stress 3%: The band structure of (a) InSe/β-Sb heterostructure, (b) β-Sb and (c) InSe sublayer, respectively. The bands plotted in red and blue in (a) denote the bands dominated by β-Sb and InSe layer, respectively. The square of transition dipole moment between the highest valence band and the lowest conduction band for (d) InSe/β-Sb heterostructure, and individual (e) β-Sb, (f) InSe layers, respectively. Photo-absorption properties of (g) InSe/β-Sb heterostructure and individual (h) β-Sb, (i) InSe layers, respectively.

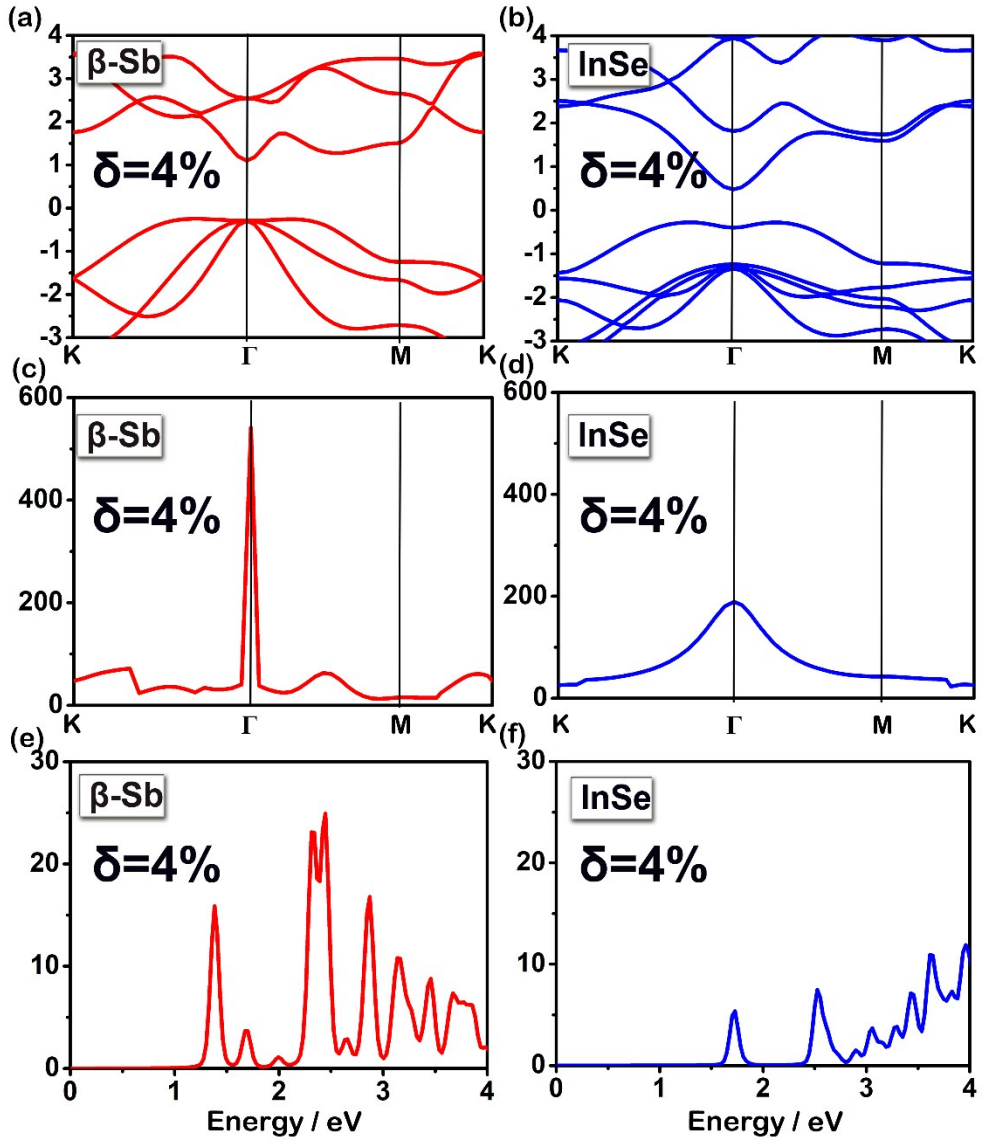


**Figure S13** Under lateral tensile stress 4%: The band structure of (a) β-Sb and (b) InSe sublayer, respectively.. The square of transition dipole moment between the highest valence band and the lowest conduction band for individual (c) β-Sb, (d) InSe layers, respectively. Photo-absorption properties of individual (e) β-Sb, (f) InSe layers, respectively.

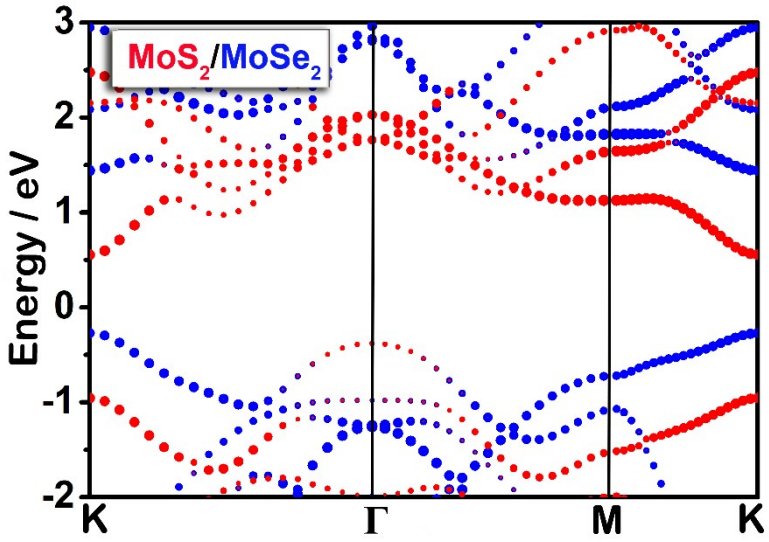


**Figure S14** Band structure of $MoS_2/MoSe_2$ heterostructure. The bands plotted in red and blue denote the bands dominated by $MoS_2$ and $MoSe_2$ layer, respectively. The Fermi level is shifted to 0 eV. The unit cell of $MoS_2$ and $MoSe_2$ are used to construct the heterostructure. The lattice parameter of $MoS_2/MoSe_2$ heterostructure is 3.23 Å, and the miss-matched rate is only 1.9%.

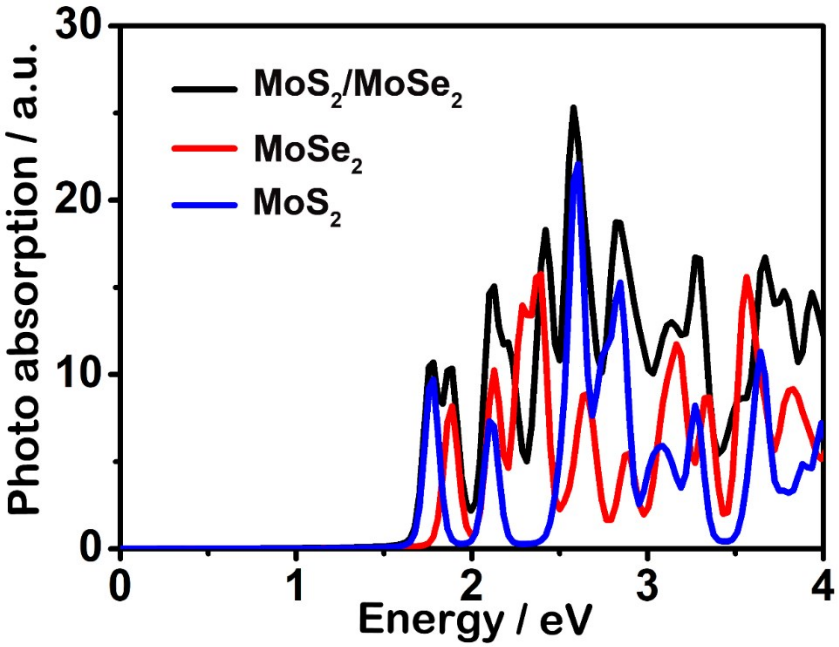


**Figure S15** Photo-absorption properties of individual $MoS_2$, $MoSe_2$ layers, and $MoS_2/MoSe_2$ heterostructure.

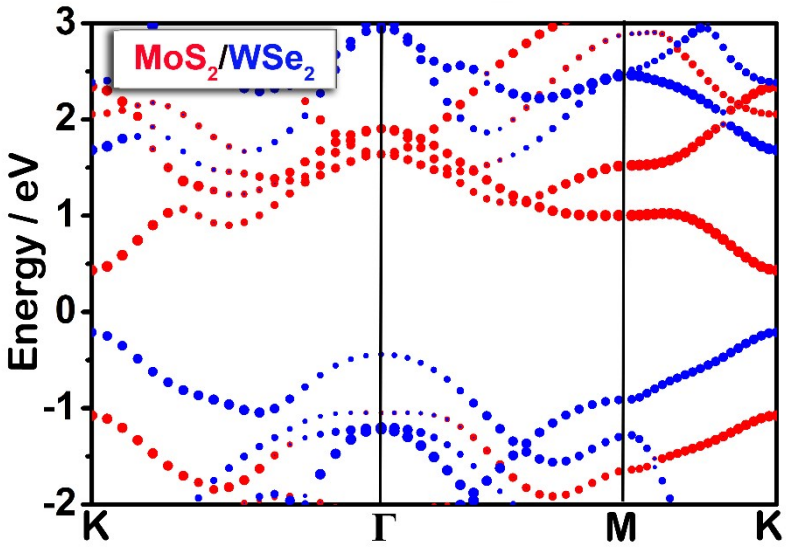


**Figure S16** Band structure of $MoS_2/WSe_2$ heterostructure. The bands plotted in red and blue denote the bands dominated by $MoS_2$ and $WSe_2$ layer, respectively. The Fermi level is shifted to 0 eV. The unit cell of $MoS_2$ and $WSe_2$ are used to construct the heterostructure. The lattice parameter of $MoS_2/WSe_2$ heterostructure is 3.23 Å, and the miss-matched rate is only 1.9%.

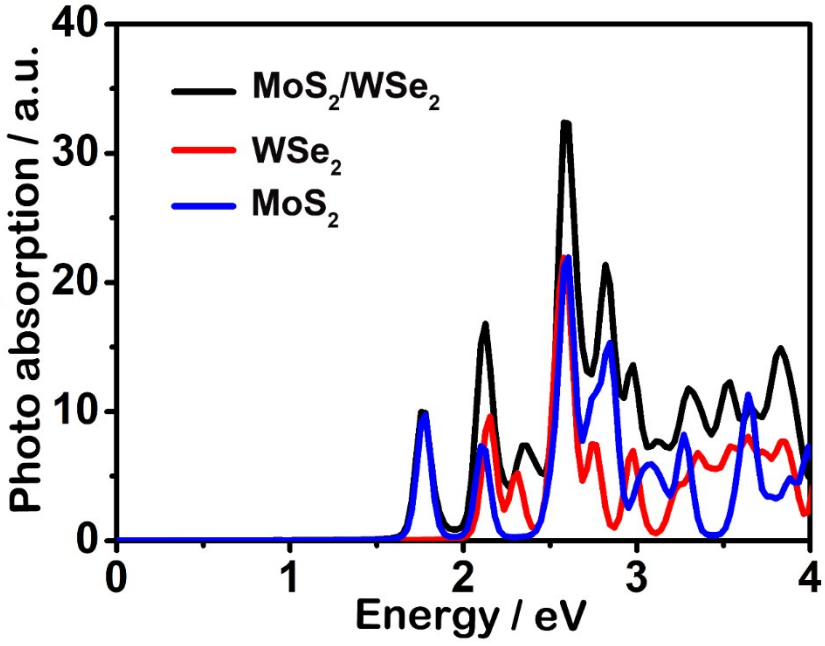


**Figure S17** Photo-absorption properties of individual $MoS_2$, $WSe_2$ layers, and $MoS_2/WSe_2$ heterostructure.

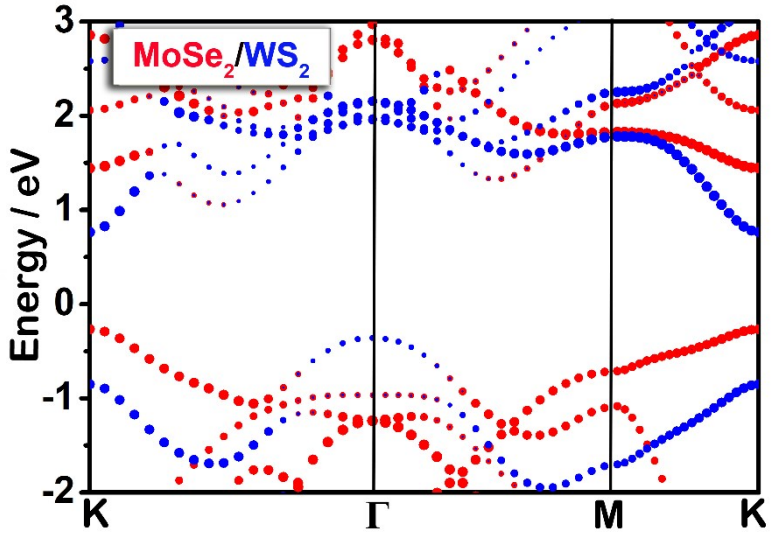


**Figure S18** Band structure of $MoSe_2/WS_2$ heterostructure. The bands plotted in red and blue denote the bands dominated by $MoSe_2$ and $WS_2$ layer, respectively. The Fermi level is shifted to 0 eV. The unit cell of $MoSe_2$ and $WS_2$ are used to construct the heterostructure. The lattice parameter of $MoSe_2/WS_2$ heterostructure is 3.23 Å, and the miss-matched rate is only 1.9%.

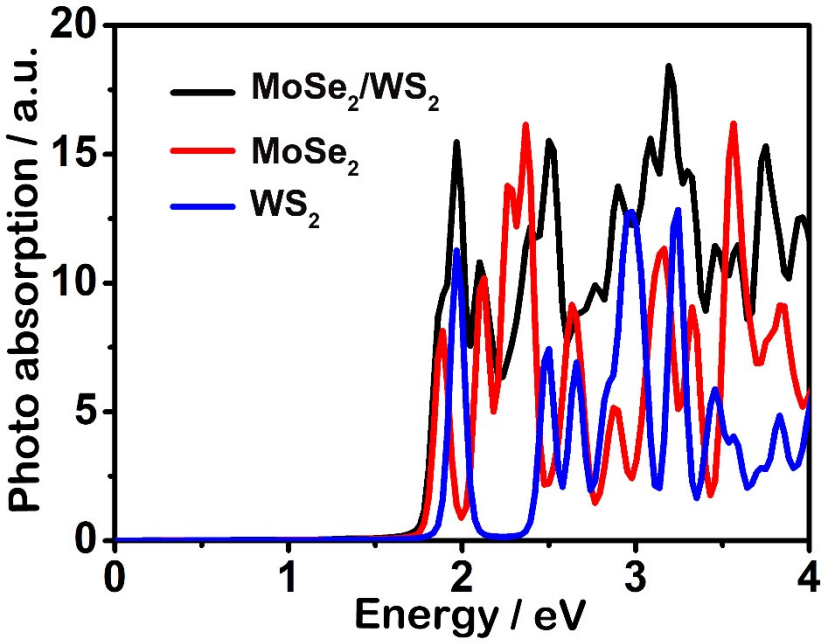


**Figure S19** Photo-absorption properties of individual $MoSe_2$, $WS_2$ layers, and $MoSe_2/WS_2$ heterostructure.

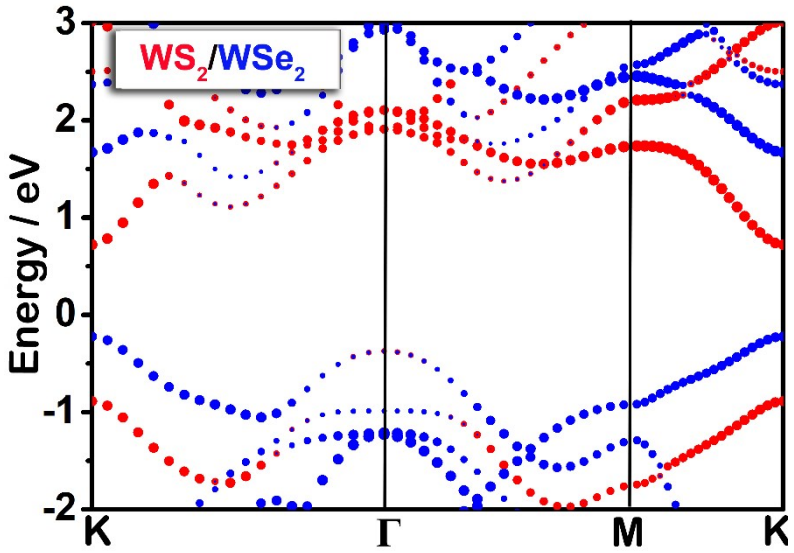


**Figure S20** Band structure of $WS_2/WSe_2$ heterostructure. The bands plotted in red and blue denote the bands dominated by $WS_2$ and $WSe_2$ layer, respectively. The Fermi level is shifted to 0 eV. The unit cell of $WS_2$ and $WSe_2$ are used to construct the heterostructure. The lattice parameter of $WS_2/WSe_2$ heterostructure is 3.23 Å, and the miss-matched rate is only 1.9%.

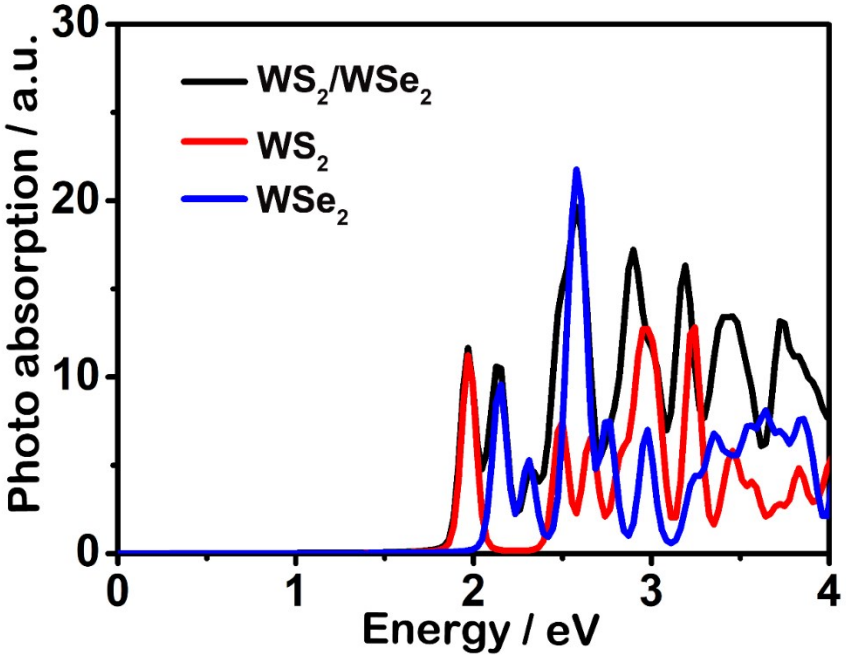


**Figure S21** Photo-absorption properties of individual $WS_2$, $WSe_2$ layers, and $WS_2/WSe_2$ heterostructure.

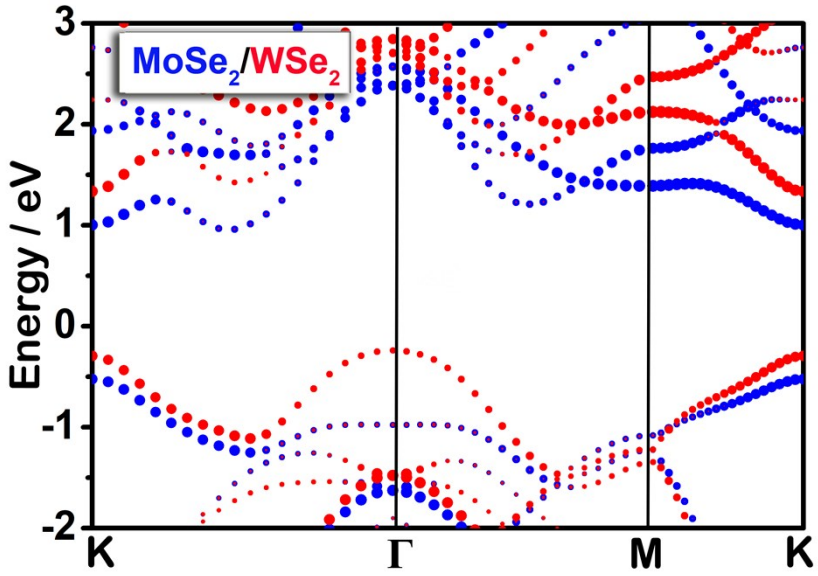


**Figure S22** Band structure of $MoSe_2/WSe_2$ heterostructure. The bands plotted in red and blue denote the bands dominated by $WS_2$ and $WSe_2$ layer, respectively. The Fermi level is shifted to 0 eV. The unit cell of $WS_2$ and $WSe_2$ are used to construct the heterostructure. The lattice parameter of $WS_2/WSe_2$ heterostructure is 3.29 Å, and there is no miss-matched rate.

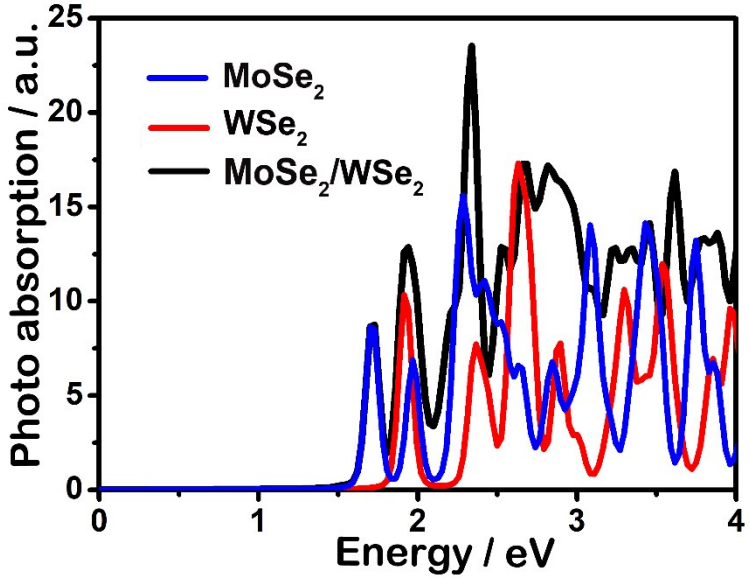


**Figure S23** Photo-absorption properties of individual $MoSe_2$, $WSe_2$ layers, and $MoSe_2/WSe_2$ heterostructure.

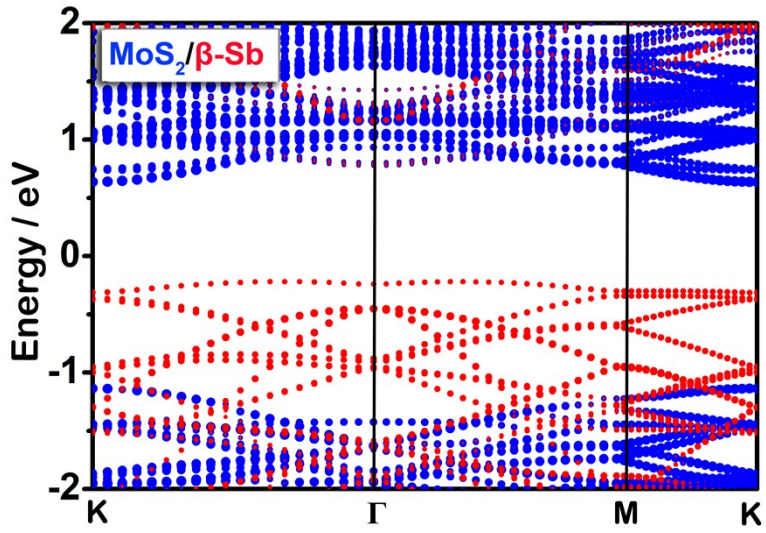


**Figure S24** Band structure of $MoS_2$/β-Sb heterostructure. The bands plotted in red and blue denote the bands dominated by β-Sb and $MoS_2$ layer, respectively. The Fermi level is shifted to 0 eV. The 3×3 supercell of β-Sb and the 4×4 supercell of $MoS_2$ are used to construct the heterostructure. The lattice parameter of $MoS_2$/β-Sb heterostructure is 12.61 Å, and the miss-matched rate is only 2%.

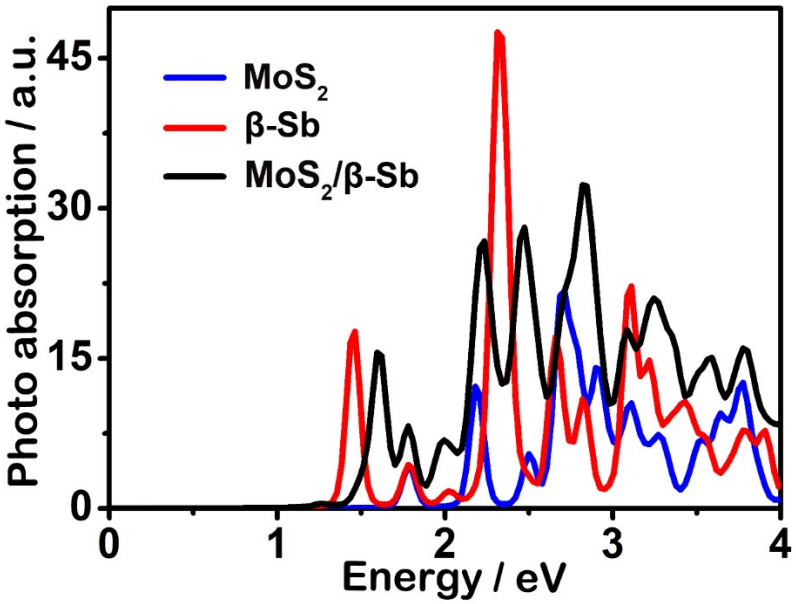


**Figure S25** Photo-absorption properties of individual $MoS_2$, β-Sb layers, and $MoS_2$/β-Sb heterostructure.

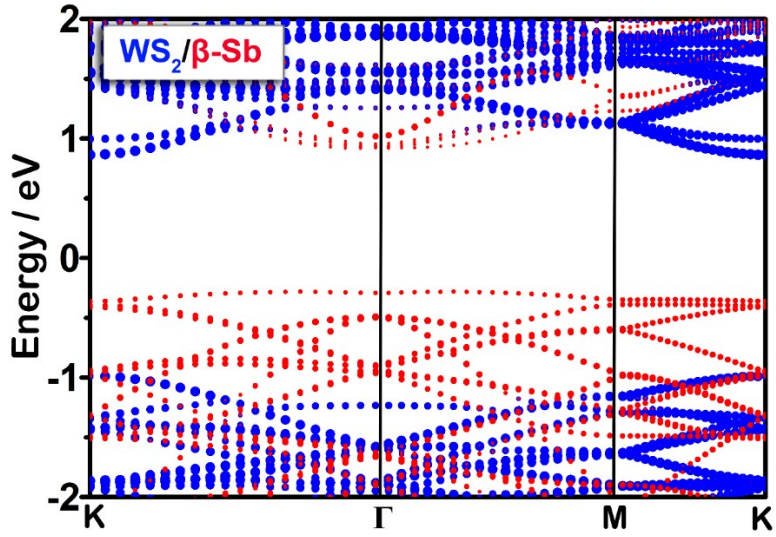


**Figure S26** Band structure of $WS_2$/β-Sb heterostructure. The bands plotted in red and blue denote the bands dominated by β-Sb and $WS_2$ layer, respectively. The Fermi level is shifted to 0 eV. The 3×3 supercell of β-Sb and the 4×4 supercell of $WS_2$ are used to construct the heterostructure. The lattice parameter of $WS_2$/β-Sb heterostructure is 12.68 Å, and the miss-matched rate is only 2.5%.

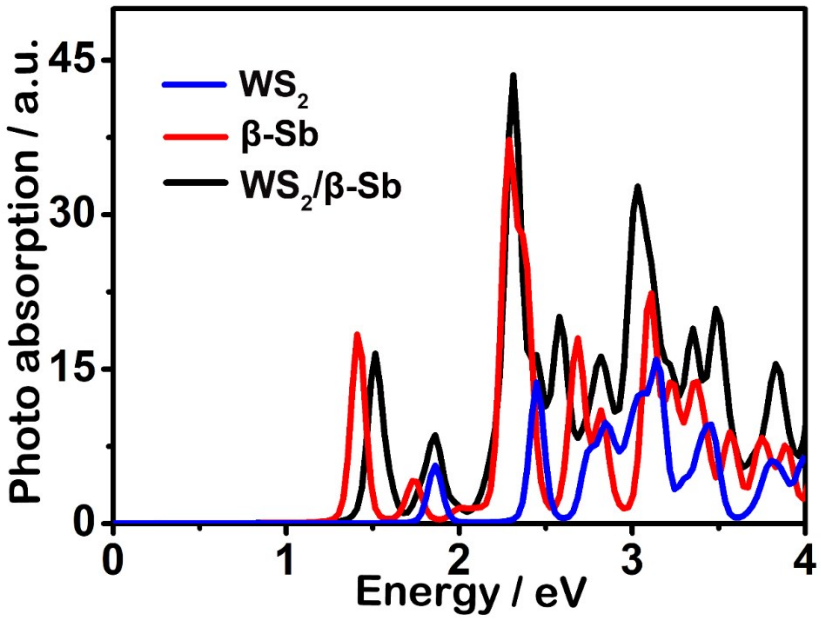


**Figure S27** Photo-absorption properties of individual $WS_2$, β-Sb layers, and $WS_2$/β-Sb heterostructure.

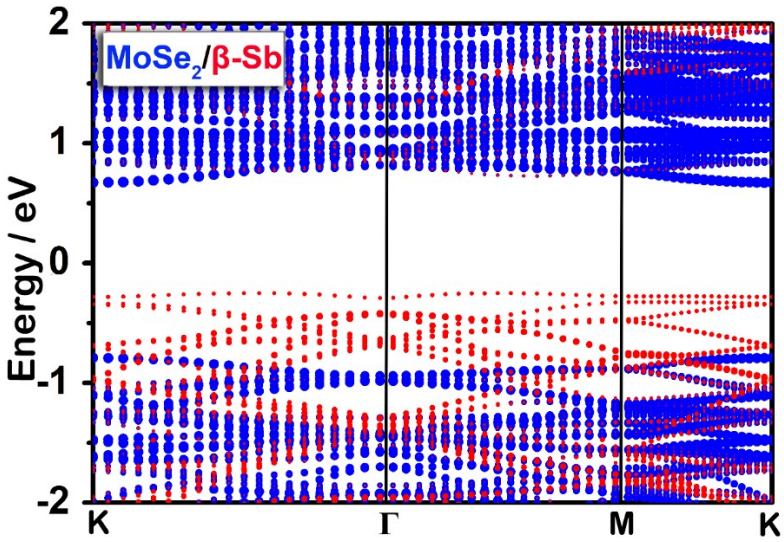


**Figure S28** Band structure of $MoSe_2$/β-Sb heterostructure. The bands plotted in red and blue denote the bands dominated by β-Sb and $MoSe_2$ layer, respectively. The Fermi level is shifted to 0 eV. The 4×4 supercell of β-Sb and the 5×5 supercell of $MoSe_2$ are used to construct the heterostructure. The lattice parameter of $MoSe_2$/β-Sb heterostructure is 16.54 Å, and the miss-matched rate is only 0.5%.

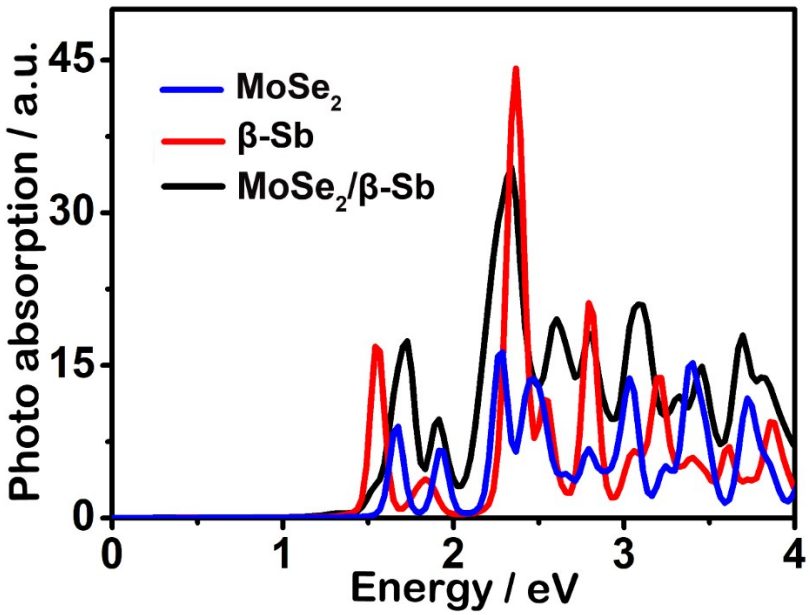


**Figure S29** Photo-absorption properties of individual $MoSe_2$, β-Sb layers, and $MoSe_2$/β-Sb heterostructure.

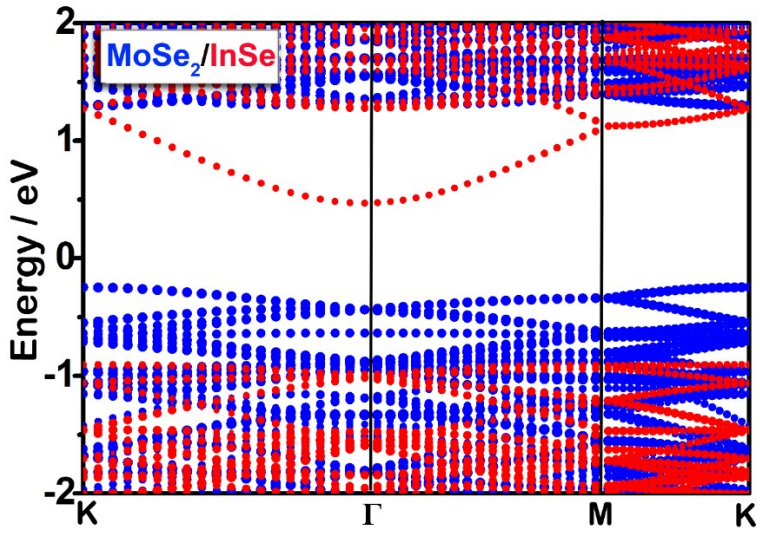


**Figure S30** Band structure of $MoSe_2$/InSe heterostructure. The bands plotted in red and blue denote the bands dominated by InSe and $MoSe_2$ layer, respectively. The Fermi level is shifted to 0 eV. The 4×4 supercell of InSe and the 5×5 supercell of $MoSe_2$ are used to construct the heterostructure. The lattice parameter of $MoSe_2$/InSe heterostructure is 16.41 Å, and the miss-matched rate is only 0.8%.

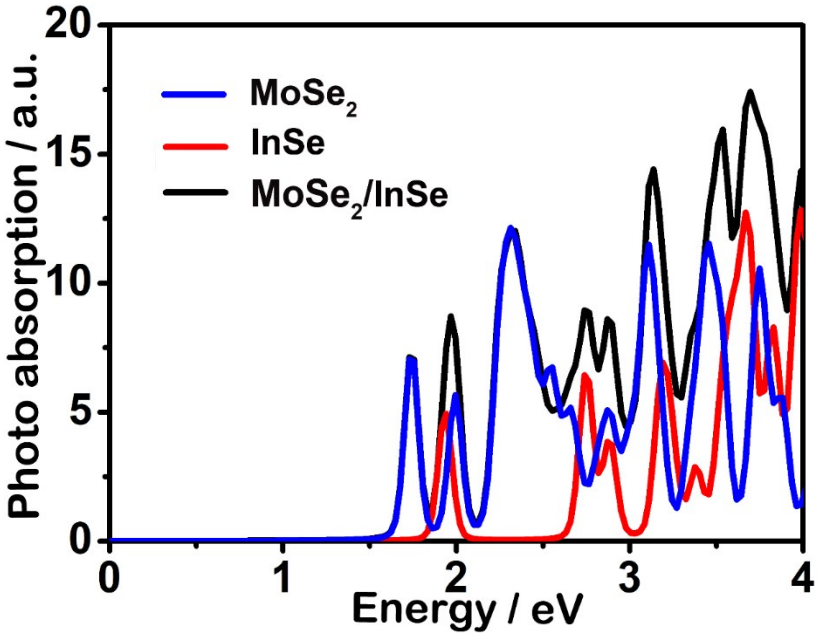


**Figure S31** Photo-absorption properties of individual $MoSe_2$, InSe layers, and $MoSe_2$/ InSe heterostructure.

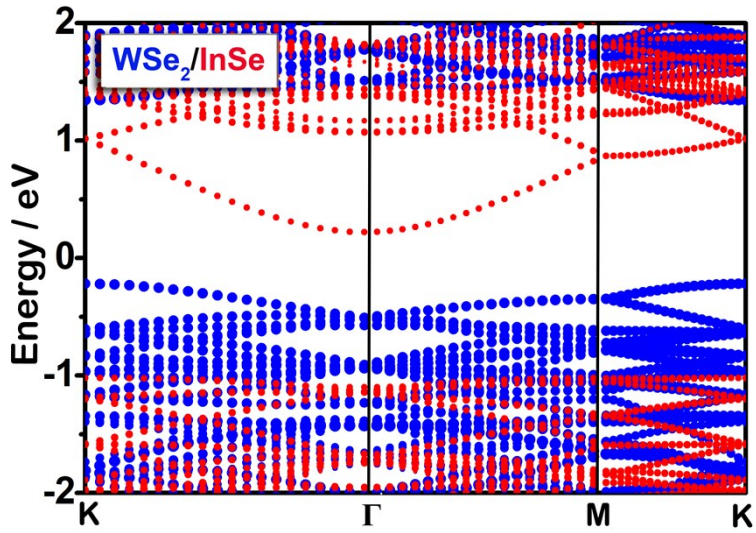


**Figure S32** Band structure of $WSe_2$/InSe heterostructure. The bands plotted in red and blue denote the bands dominated by InSe and $WSe_2$ layer, respectively. The Fermi level is shifted to 0 eV. The 4×4 supercell of InSe and the 5×5 supercell of $WSe_2$ are used to construct the heterostructure. The lattice parameter of $WSe_2$/InSe heterostructure is 16.50 Å, and the miss-matched rate is only 1.3%.

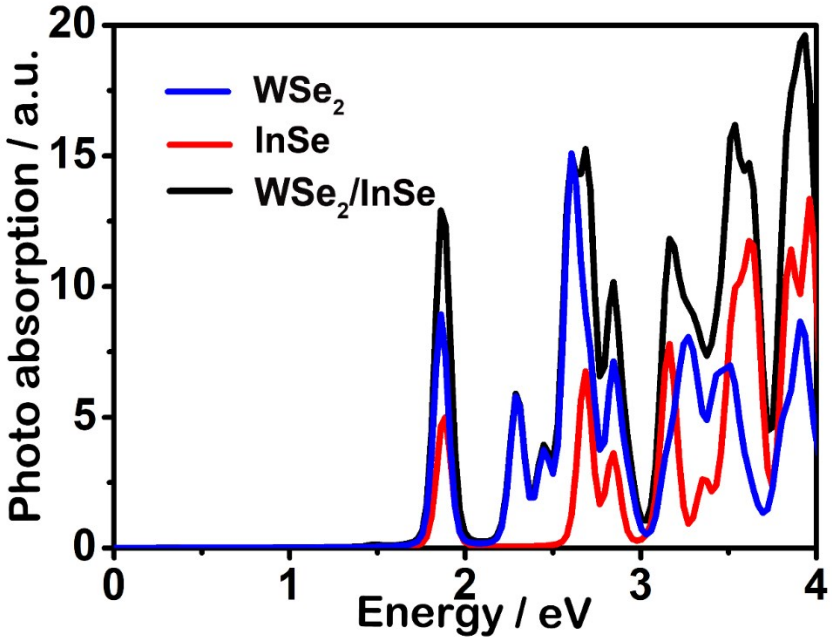


**Figure S33** Photo-absorption properties of individual $WSe_2$, InSe layers, and $WSe_2$/InSe heterostructure.

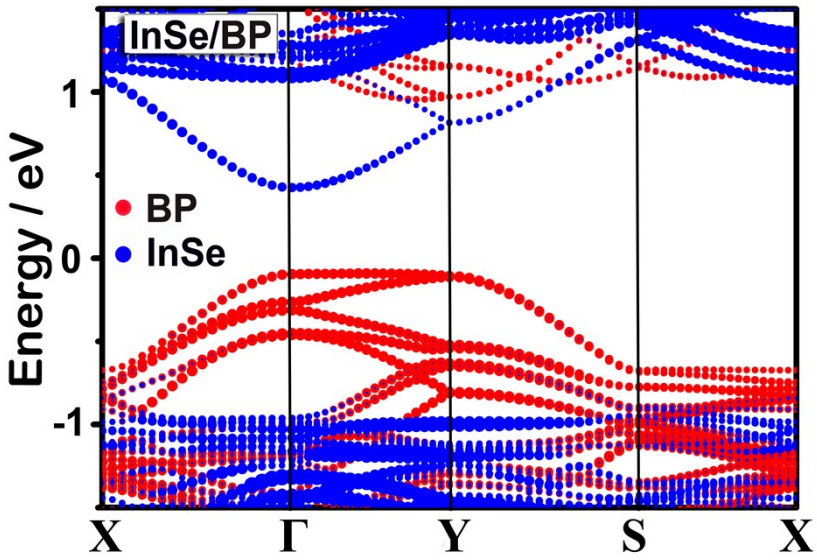


**Figure S34** Band structure of InSe/BP heterostructure. The bands plotted in red and blue denote the bands dominated by BP and InSe layer, respectively. The Fermi level is shifted to 0 eV. The rectangular supercell cell is constructed using a 3×5 unit rectangular cell of BP and a 2×4 unit rectangular cell of InSe to minimize the lattice mismatch. The lattice parameters of the BP/InSe supercell are determined as 13.8 and 16.4 Å in the x and y directions, respectively, which induces a maximum strain in both the BP and InSe lattices of ~2%.

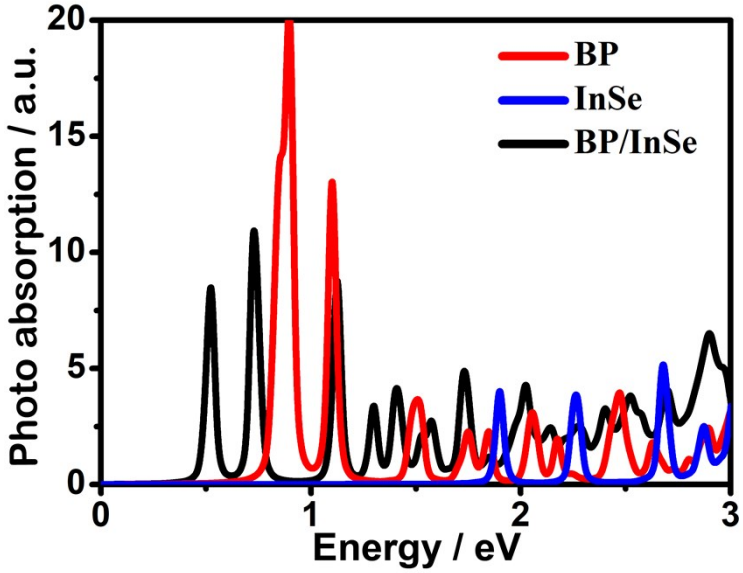


**Figure S35** Photo-absorption properties of individual InSe, BP layers, and InSe/BP heterostructure.

To explore optical properties, we employ the energy-dependent dielectric functions to investigate the optical absorption of isolate InSe, β-Sb layer, and InSe/β-Sb heterostructure. The dielectric matrix is determined by the following equation, [1]

$$\varepsilon_{\alpha\beta}(\omega) = \frac{4\pi^2 e^2}{\Omega} \lim_{q\to 0} \frac{1}{q^2} \sum_{c,v,\mathbf{k}} 2w_{\mathbf{k}} \delta(\varepsilon_{c\mathbf{k}} - \varepsilon_{v\mathbf{k}} - \omega) \times \left\langle u_{c\mathbf{k}+e_\alpha \mathbf{q}} \mid u_{v\mathbf{k}} \right\rangle \left\langle u_{c\mathbf{k}+e_\beta \mathbf{q}} \mid u_{v\mathbf{k}} \right\rangle * \quad (1)$$

Where Ω is the volume of the primitive cell, q is the electron momentum operator, v and c are the valence and conduction band states, respectively, $\omega_k$ is the k point weight, $\varepsilon_{ck}$, $\varepsilon_{vk}$ and $\mu_{ck}$, $\mu_{vk}$ are the eigenvalues and wave-functions at the k point, respectively, and $e_\alpha$, $e_\beta$ are the unit vectors for the three Cartesian directions.

The binding energy is defined as $E_b = E_{InSe} + E_{\beta\text{-}Sb} - E_{InSe/\beta\text{-}Sb}$, where, $E_{InSe}$, $E_{\beta\text{-}Sb}$ and $E_{InSe/\beta\text{-}Sb}$ represent the total energy of isolated InSe and β-Sb monolayer, and InSe/β-Sb heterostructure, respectively.

## References

1 Gajdoš, M., Hummer, K., Kresse, G., Furthmüller, J. & Bechstedt, F. Linear Optical Properties in The Projector-augmented Wave Methodology. *Phys. Rev. B* **73**, 045112 (2006).